ORIGINAL PAPER

Joris Proost · **Michael Baklanov**
Rita Verbeeck · **Karen Maex**

Morphology of corrosion pits in aluminum thin film metallizations

Abstract The morphology of corrosion pits in sputtered pure aluminum and Al(0.5 wt% Cu) thin film metallizations has been investigated for a diluted chloride solution. The observed fractal-like patterns show clearly distinct features in ramification and branch density, which can be attributed to microscopic inhomogeneities inside the aluminum film. It is discussed how these observations may have an impact on the current description of diffusion phenomena in thin films, e.g. concerning electromigration.

Key words Pitting · Fractal · Aluminum · Metallization

Introduction

Pitting corrosion has already been studied quite extensively for bulk materials because of its immense practical importance [1]. It is characteristic for metals possessing a thin protective oxide film (e.g. stainless steel, aluminum, titanium, etc.). The breakdown of this passive film may be initiated purely chemically, if the concentration of aggressive anions (e.g. Cl^-) exceeds a critical value, depending on the nature of both metal and anion. But usually pits start to grow at chemical impurities or inclusions or, in the case of extremely pure metals, at physical defects like dislocations. Once the pit growth has started, the composition of the electrolyte changes locally because of the metal dissolution. The hydrolysis of metal ions further increases the aggressiveness of the medium close to the dissolution site, leading to the acceleration of the corrosion process. The propagation of the pit is controlled by the relative rate of metal dissolution and ionic transport in the liquid phase. When the electrolyte becomes saturated, salt may precipitate on the pit wall, leading to an abrupt cessation of the pit growth process. Alternatively, if the concentration of aggressive anions decreases significantly in the vicinity of a dissolution site, the bare metal surface may oxidize. For stable pit growth, when corrosion lasts indefinitely in time, a balance is to be maintained between the metal dissolution and the ionic transport towards and away from the active surface.

Recently, results were published on the morphology of corrosion pits in 50-nm evaporated pure aluminum films [2]. It was shown that, for specific Cl^- and Fe^{3+} concentrations, a fractal-like corrosion pattern was obtained. The influence of the two ionic concentrations was explained by the balance between anodic and cathodic processes under open-circuit conditions. The anodic area and hence the corrosion current steadily increases with time, which must be compensated by cathodic processes. Hydrogen evolution at the fresh metal surface is one possibility, but can be considered to be transport limited [3]. An increase in the active anodic area must therefore be sustained by additional cathodic reactions such as the reduction of Fe^{3+}. Since the area available for these reactions is a slowly decreasing function of time, the corrosion current cannot be increased further once all the cathodic reactions become transport limited, leading to a natural limit for the anodic current. This limiting current was believed to increase with the concentration of Fe^{3+} ions, resulting in a circular growth front. At low Cl^- concentrations the active surface is distributed over several individual growth regions, which propagate randomly in the film. At high Cl^- concentration dense pitting structures are produced.

The main purpose of this paper is to investigate the origin of the pit profile ramification. According to Balazs and Gouyet [2], this is caused by hydrogen gas evolution, which locally induces strong convection in the electrolyte and leads to the dilution of the liquid in the vicinity of the active metal surface. It can then be expected that the role of hydrogen bubbling in the pitting morphology diminishes with increasing Cl^- concentra-

J. Proost (⊠) · M. Baklanov · R. Verbeeck · K. Maex
Imec, Kapeldreef 75, B-3001 Leuven, Belgium
Tel.: +32-16-281 488; Fax: +32-16-281 214
e-mail: proost@imec.be

tion, which they indeed observed. On the other hand, it is not unlikely that the pit profile ramification is caused directly by microscopic inhomogeneities in the metal film itself, e.g. due to its grain structure. In this case, differences in the intra- and intergranular dissolution rate will also be less pronounced at high Cl^- concentration. The diffusion of active ionic species, leading to the dissolution of specific metal ions, may then be described by a fractal pattern determined directly by structural features in the aluminum film. The study of pitting corrosion may then turn out to be very relevant to the identification of preferential diffusion paths [4] in aluminum thin films. This is of particular interest in microelectronic applications, where Al and its alloys are widely used for metallization. The diffusion of Al, forced by the high current densities and known as electromigration, is considered a main failure mechanism for integrated circuits and is largely documented both theoretically and experimentally to be a function of microstructure as well [5]. Therefore, the idea of this work is to study the morphology of corrosion pits in aluminum films, not as a function of ionic concentrations in the electrolyte as was done in [2], but as a function of film microstructure.

Experimental

Both pure Al (5N5) and Al(0.5 wt% Cu) films were sputter deposited from semiconductor-grade targets in a Balzers CLC9000 cluster tool (base pressure 10^{-8} Torr) on 6-inch Si wafers covered with 500 nm PECVD SiO_2. In order to vary the microstructure, films were sputtered 50 nm thick at 100, 200, 300 and 400 °C. Varying the deposition temperature was preferred to a post-deposition anneal, since this can seriously reduce the surface oxide integrity and hence alter the pitting mechanism [6]. In all cases, 4×5 cm² samples were marked onto the Si substrate and cleaved by hand out of the wafer with a diamond-tipped cutting tool.

All experiments were carried out under open-circuit conditions in 500 ml of stagnant electrolyte, which was prepared from reagent-

Fig. 1a, b SEM images of 50-nm pure Al films as deposited at 100 °C (*left*) and 400 °C (*right*)

grade chemicals and deionized water. The concentration of Cl^- and Fe^{3+} ions was kept constant at 10 mM and 0.2 mM respectively. This was done by dissolving the appropriate amount of NaCl and $Fe_2(SO_4)_3$ in a 5 mM sulphuric acid solution, resulting in a bulk pH of 2.5. After immersion, samples were vigorously stirred in deionized water and dried in a dry nitrogen stream.

Microscopic images of the corrosion pits were taken with an optical microsope (OM) used in the Nomarsky interference mode. More detailed, back-scattered SEM analysis was carried out at an accelerating voltage of 1.2 kV, with an angle of 30° from normal incidence. A standard θ–2θ X-ray diffraction scan was used to check the crystallinity of the films. The surface of the sputtered films was analyzed with X-ray Photoelectron Spectroscopy (XPS), applying Al Kα radiation of 1486.6 eV and using an SSX-100 spectrometer and a concentric hemispherical analyzer.

Results and discussion

Characterization of as-deposited films

The effect of varying the substrate temperature during sputtering of the 50-nm films is most obvious from the SEM images in Fig. 1. As opposed to the other films, no continuous layer could be obtained at 400 °C, where an infinite resistivity was measured. This is related with the bad wetting of sputtered Al onto SiO_2 films, which becomes especially pronounced at elevated temperatures [7]. All films were polycrystalline, with a preferred {111} texture as obtained from the XRD patterns.

XPS analysis on a continuous pure Al film was carried out to estimate the thickness of the native oxide after deposition. Assuming a simple overlayer model with an Al substrate covered by a thin Al_2O_3 layer and implementing the appropriate literature values [8], the following formula is obtained for the oxide thickness in our experimental set-up:
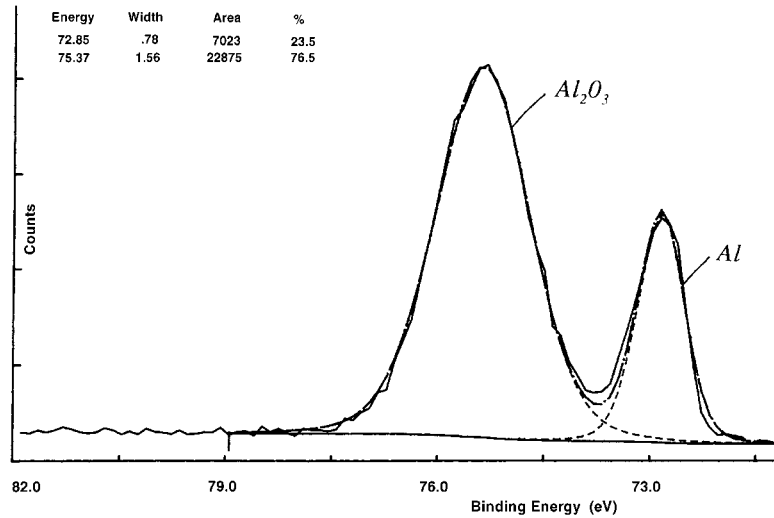
$$d_{ox} = 14,2 \text{Å} \ln \left(1.01 \frac{I_{ox}}{I_m} + 1 \right)$$

with I_{ox} and I_m the peak area of the oxidized and elemental Al2p fraction respectively. Based on the results of Fig. 2, an oxide thickness of 21 Å is calculated.

a

b
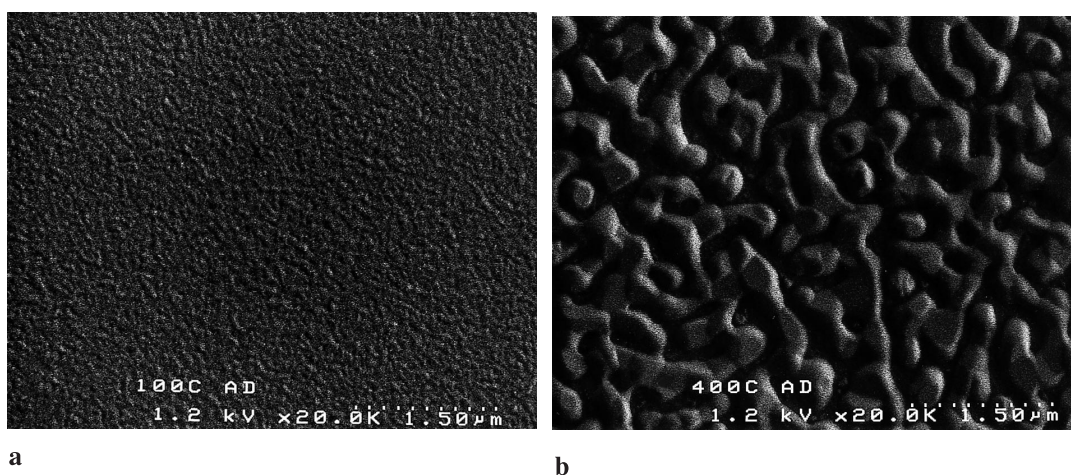
Fig. 2 Detailed spectrum from XPS on surface of 800-nm pure Al film

| Energy	Width	Area	%
72.85	.78	7023	23.5
75.37	1.56	22875	76.5

Pit morphology in pure Al films

All samples of 50-nm pure Al were immersed together for 15 min in stagnant electrolyte. The pit morphologies as observed in the OM are shown in Fig. 3. In all cases, fractal-like patterns are obtained. There is a notable difference between the film sputtered at 400 °C and the other sputtered films. The first shows a clear tendency towards circular growth. For the film deposited at 300 °C, the density of the branches is less than that of the films deposited at 100 °C and 200 °C. Since all films were immersed together in exactly the same solution, the same concentrations are to be considered for every sample. Because of the relatively large amount of elec-

Fig. 3a–d Pit morphologies as observed by OM on 50-nm pure Al films sputtered at 100, 200, 300 and 400 °C

a 100° C

c 200° C

b 300° C

d 400° C
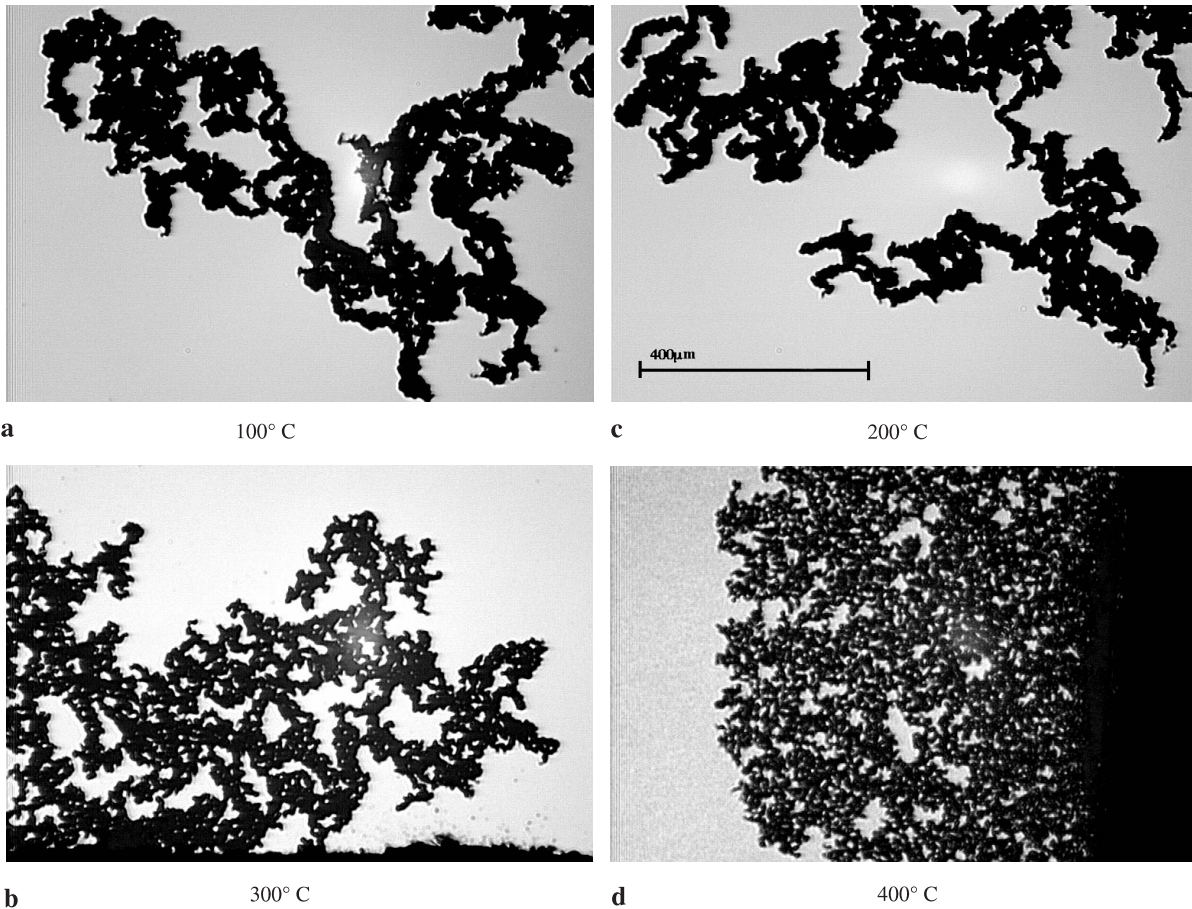
trolyte, no interaction can be assumed between the different samples. Also, within the area of one film, no interaction was assumed between the pitting at different locations. Therefore, the observed differences in pit morphology should be attributed entirely to microstructural differences.

For the film deposited at 400 °C, the most striking feature is its non-continuity (cf. Fig. 1), resulting in a significant increase in surface area as compared to continuous films. This basically has the same effect on the limiting current as increasing the Fe^{3+} concentration, resulting in the observed circular growth front.

Concerning the films sputtered at 100, 200 and 300 °C, the influence of grain size or, more fundamentally, of the effective grain boundary area on pitting susceptibility should be considered. For the film sputtered at 400 °C, the non-continuity is believed to have a much bigger impact. At grain boundaries, a discontinuity in the oxide layer is introduced [9]. This may be the result of different grain orientations or cathodic impurities that preferentially segregate to the grain boundaries during deposition. Grain boundaries have also been described as regions where the oxide layer is virtually non-existent or in a state in which it is electrically and/or structurally weak [10]. It seems very plausible indeed to ascribe the reduced branch density for the 300 °C sample to the reduced grain boundary area. Its effect is at least qualitatively the same as that of decreasing the Cl^- concentration. This is what can be expected, since enhancing the pitting probability essentially can be achieved both by increasing the Cl^- concentration and increasing the area of potential pitting places (grain boundaries). The fact that no qualitative difference is observed between the films sputtered at 100 °C and 200 °C is probably because the effect of grain size is not so marked in this temperature range. Because of the exponential Arrhenius dependence of

Fig. 5a–h Pit morphologies as observed by OM on 50-nm Al(0.5 wt % Cu) films (*left*) and pure Al films (*right*), deposited at 100, 200, 300 and 400 °C. Note the different scale from that of Fig. 3

grain size on deposition temperature, the temperature effect will indeed be more pronounced between 200 °C and 300 °C.

The crucial role of grain structure becomes even more evident from SEM inspection, shown in Fig. 4. It can be clearly seen that the pitting process very selectively removes some grains, while leaving others totally undissolved. This provides direct evidence that the pit profile ramification is determined primarily by microscopic inhomogenities. Their exact nature still needs further investigation in terms of grain size distribution and grain boundary structure. In the next paragraph, the extent to which this specific microstructural selectivity is influenced by the addition of Cu is investigated.

## Pit morphology in Al(0.5 wt% Cu) films

The pit morphologies for the 50-nm sputtered Al(0.5 wt% Cu) films after a 15 min immersion are shown in Fig. 5. The morphologies for the pure Al films are again included as a reference, but with a higher magnification than in Fig. 3. Compared to these 50-nm pure Al films, the pit morphology for the film deposited at 400 °C is quite similar, indicating that it is again fully governed by the film non-continuity. The differences between the films deposited at 100, 200 and 300 °C, however, are more pronounced than for the pure Al films. Apart from grain structure, the addition of Cu has to be considered here as well, since this is known to alter the pitting corrosion susceptibility to a great extent [11]. Results on Al(2% Cu) films [9] showed that due to the formation of the equilibrium $CuAl_2$ θ-phase, defects or discontinuities at or near these incoherent precipitates can cause localized breaks in the oxide layer, leading to an increased pitting probability. The Cu-rich precipitates also act as more efficient cathodic reduction sites, thereby increasing the corrosion reaction rate. During sputtering at

Fig. 4a, b SEM images of pit morphology on a 800-nm thick Al film. The pitting process very selectively removes some grains, while leaving others totally undissolved
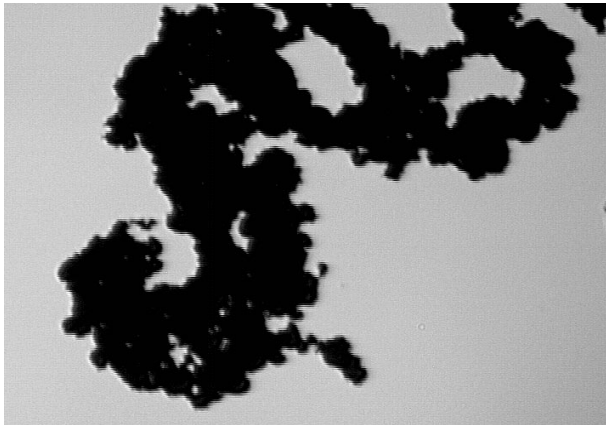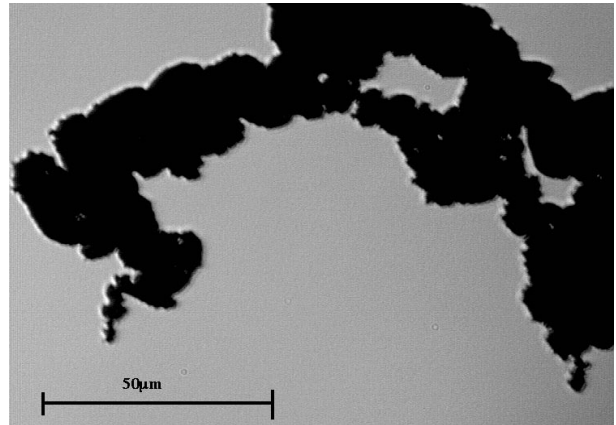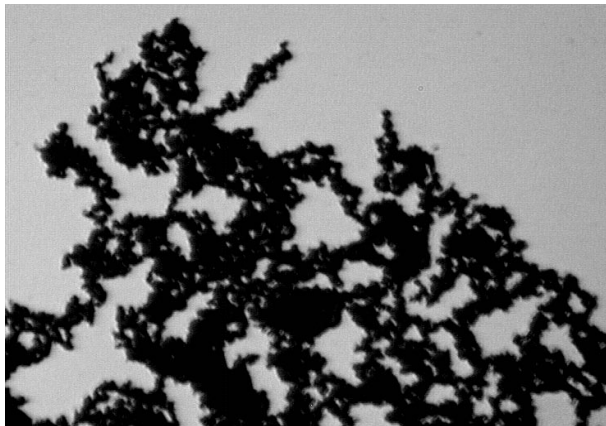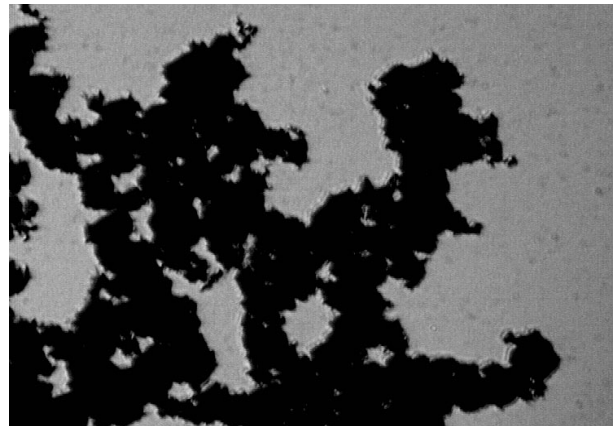

a

b

a   100° C   b

c   200° C   d
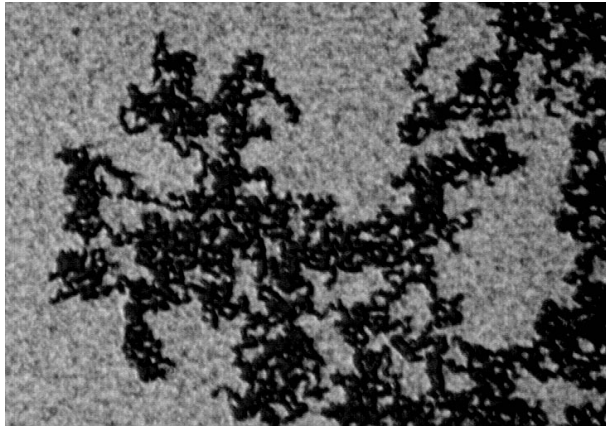
50μm
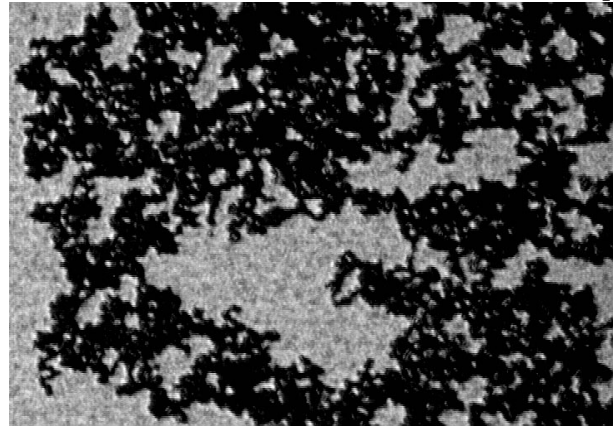
e   300° C   f

g   400° C   h
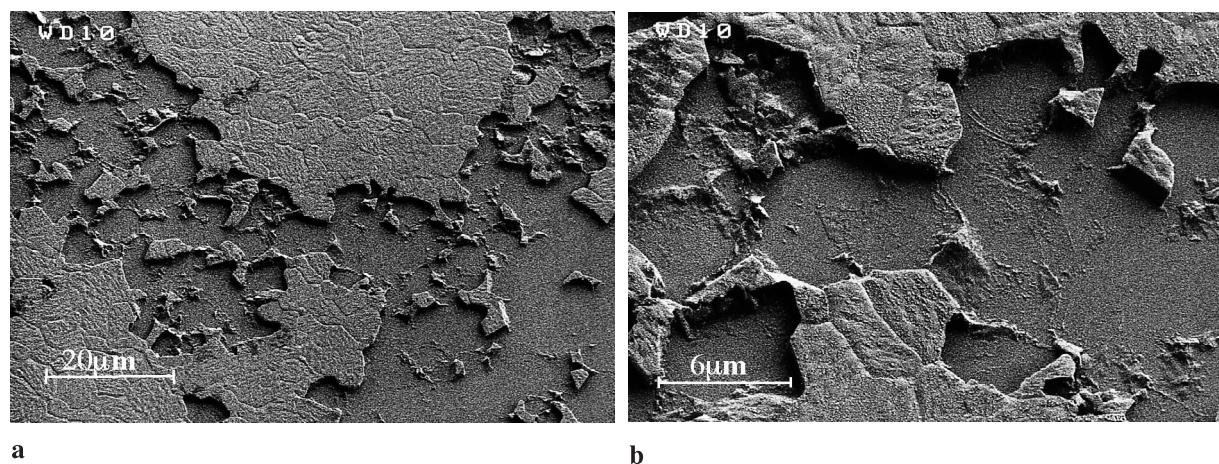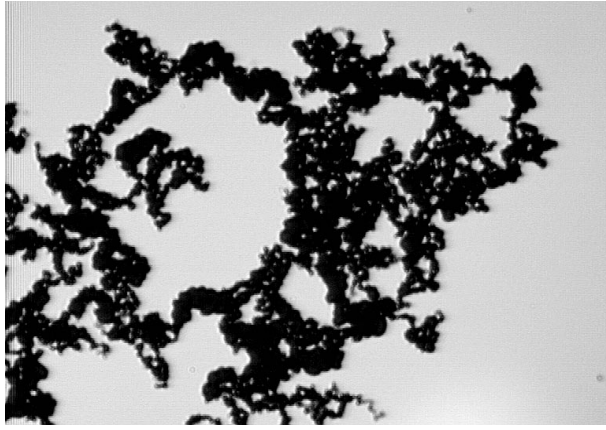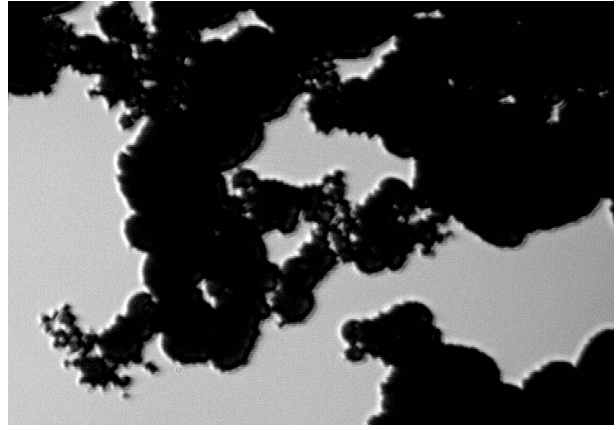
200 °C, larger θ-precipitates than those obtained by deposition at 100 °C will be formed. Based on literature data for 100-nm Al(3% Cu) films [12], θ-precipitation is not even expected during sputtering at 100 °C. Instead, the metastable θ' or even θ''-phase will precipitate, which will have a less detrimental impact on the integrity of the native oxide because of their (semi-) coherency and small size ($\leq$10 nm diameter [12]). Sputtering at 300 °C would, according to the phase diagram [13], be at the edge of the solubility limit, which greatly reduces the impact of Cu on the pitting corrosion susceptibility.

These microstructural observations seem to be very relevant for explaining our observed differences in pit morphology. The density of the branches in the fractal-like patterns is the highest for the film deposited at 200 °C. This can be attributed to the presence of the most vulnerable θ-precipitates, which were indeed observed in plan-view TEM after deposition at 200 °C [14]. When assuming most of the Cu in solution for the sample sputtered at 300 °C, its pitting behavior should resemble that of pure Al, provided both films have similar grain sizes (which is indeed expected when Cu is in solution). However, a decreased density is observed for Al(Cu). And if the precipitation in the 100 °C films is indeed restricted to θ' or θ'' and their effect on oxide integrity is negligible, the same decrease in branch density holds for this sample as compared to the pure Al film deposited at 100 °C. A similar trend but on totally different morphologies was found by Griffin et al. [9] while comparing anodically polarized 1-µm pure Al and Al(Cu) films in a 40 mM NH_4Cl aqueous solution. The authors stated that "the tortuous paths and the increased serrations in the Al(2% Cu) films are indicative of the structural features of the alloy". Our observations using specific pitting solutions revealed the same microstructural features, different from grain size or θ-precipitation. Their exact nature is not yet understood, but at least seems to indicate that the addition of Cu, introducing additional microstructural inhomogeneities, again determines the pit profile ramification.

Conclusions

We have described the pit morphologies obtained in a very specific electrolyte for both pure aluminum and Al(0.5 wt% Cu) thin film metallizations, deposited at different temperatures. Fractal-like patterns are observed in all cases. Their clearly distinct features in ramification and branch density could be partly explained by the specific influence of grain size and Cu precipitation on the pitting mechanism itself. However

SEM inspection showed the pitting process to be very selective towards the grain structure, leaving some grains totally undissolved. Also, the addition of Cu seemed to affect the fractal morphology, apart from the effect of precipitation. These arguments provide direct evidence that the pit profile is determined primarily by microscopic inhomogeneities inside the aluminum film. Their exact nature still needs further investigation in terms of grain size distribution and grain boundary structure.

Considering the fractal-like patterns to be indicative of preferential diffusion paths in aluminum, as suggested by Sapoval et al. [4], these observations may have a large impact on the current description of diffusion phenomena in thin Al films, e.g. concerning electromigration. Despite the extensive theoretical and experimental investigations over the last three decades (recently reviewed for instance by C.-K. Hu et al. [15]), the classical kinetic approach did not allow a satisfactory understanding and control of the electromigration failure mechanism. We believe that a new approach based on a percolation-type behavior of both electromigration-induced mass and charge transport may be more effective for a general description of experimental observations.

References

1. Mansfeld F (1987) Corrosion mechanisms. Dekker, New York
2. Balazs L, Gouyet J-F (1995) Physica A 217: 319
3. Frankel GS (1990) Corros Sci 30: 1203
4. Sapoval B, Rosso M, Gouyet J-F (1989) In: Avnir D (ed) The fractal approach to heterogeneous chemistry. Wiley, New York, pp 227–245
5. Gupta D (1988) Diffusion phenomena in thin films and microelectronic materials. Noyes, Park Bridge, N.J.
6. Hernandez SE, Griffin AJ, Brotzen FR, Dunn CF (1995) J Electrochem Soc 142: 1215
7. Inoue M, Hashizume K, Tsuchikawa H (1988) J Vac Sci Technol A 6: 1636
8. Olefjord I, Mathieu HJ, Marcus P (1990) Surf Interf Anal 15: 681
9. Griffin AJ, Brotzen FR, McPherson JW, Dunn CF (1992) Proc IEEE/IRPS 239
10. Scully JR, Frankenthal RP, Hanson KJ, Siconolfi DJ, Sinclair JD (1990) J Electrochem Soc 137: 1365
11. Muller IL, Galvele JR (1977) Corros Sci 17: 179
12. Mader S, Herd S (1972) Thin Solid Films 10: 377
13. Hatch JE (1984) Aluminum, properties and physical metallurgy. ASM, Metal Parks, Ohio
14. Proost J, Witvrouw A, Cosemans P, Roussel Ph, Maex K (1997) Microelectr Eng 33: 137
15. Hu C-K, Rodbell KP, Sullivan TD, Lee KY, Bouldin DP (1995) IBM J Res Develop 39: 465